Atmos. Chem. Phys. Discuss., 11, 11007–11038, 2011
www.atmos-chem-phys-discuss.net/11/11007/2011/
doi:10.5194/acpd-11-11007-2011

Atmospheric Chemistry and Physics Discussions

Studies of propane flame soot acting as heterogeneous ice nuclei in conjunction with single particle soot photometer measurements

I. Crawford[1], **O. Möhler**[2], **M. Schnaiter**[2], **H. Saathoff**[2], **D. Liu**[1], **G. McMeeking**[1,*], **M. Flynn**[1], **K. N. Bower**[1], **P. J. Connolly**[1], **M. W. Gallagher**[1], **and H. Coe**[1]

[1]Centre for Atmospheric Science, School of Earth, Atmospheric and Environmental Sciences, University of Manchester, M13 9PL, Manchester, UK
[2]Institute for Meteorology and Climate Research, Karlsruhe Institute of Technology, Postfach 3640, 76021 Karlsruhe, Germany
[*]now at: Department of Atmospheric Science, Colorado State University, Fort Collins, Colorado, USA

Received: 1 March 2011 – Accepted: 23 March 2011 – Published: 8 April 2011

Correspondence to: I. Crawford (i.crawford@manchester.ac.uk)

Published by Copernicus Publications on behalf of the European Geosciences Union.

Abstract

The ice nucleation efficiency of propane flame soot particles with and without a sulphuric acid coating was investigated using the aerosol and cloud chamber facility AIDA (Aerosol Interaction and Dynamics in the Atmosphere). The test soot for cloud formation simulations was produced using a propane flame Combustion Aerosol Standard generator (CAST, Jing-CAST Technologies). The organic carbon content (OC) of the test soot was altered in a reproducible fashion by changing the fuel/air mixture of the generator. The soot content of ice nuclei was subsequently investigated using a combination of a pumped counterflow virtual impactor (PCVI) to separate and evaporate the ice crystals, and a DMT single particle soot photometer (SP2) to examine the mixing state of the BC containing ice residuals.

Ice nucleation was found to be most efficient for uncoated soot of low organic carbon content (~5% organic carbon content) where deposition freezing occurred at an ice saturation ratio S_{ice} ~1.22 at a temperature T = 226.6 K with 25% of the test soot becoming active as ice nuclei. Propane flame soot of higher organic carbon content (~30% and ~70% organic carbon content) showed significantly lower ice nucleation efficiency (an activated fraction of the order of a few percent in the experiments) than the low organic carbon content soot, with water saturation being required for freezing to occur. Ice nucleation occurred over the range S_{ice} = 1.22–1.70, and T = 223.2–226.6 K. Analysis of the SP2 data showed that the 5% organic carbon content soot had an undetectable OC coating whereas the 30% organic carbon content soot had a thicker or less volatile OC coating.

The application of a sulphuric acid coating to the flame soot shifted the threshold of the onset of freezing towards that of the homogeneous freezing of sulphuric acid; for the minimum OC flame soot this inhibited nucleation since the onset of freezing occurred at colder temperatures and required a greater ice saturation ratio; for the medium and maximum OC flame soot, the addition of a sulphuric acid significantly reduced the freezing threshold.

ACPD

11, 11007–11038, 2011

1 Introduction

Many studies of cirrus and orographic cloud formation have focussed on the homogeneous freezing of supercooled sulphuric acid droplets as the major mechanism (Archuleta et al., 2005; Field et al., 2001; Haag et al., 2003; Heymsfield and Miloshevich, 1993; Heymsfield and Sabin, 1989; Jensen et al., 1998; Marti and Mauersberger, 1993; Sassen and Dodd, 1988; Tabazadeh et al., 1997). Numerical parameterisations have been developed to estimate the ice crystal number concentration and size for given conditions, and solutes, which can then be used to determine cloud radiative properties (Kärcher, 2002; Kärcher and Lohmann, 2003; Koop et al., 2000; Lohmann, 2002b). However, many field studies have shown cirrus formation via heterogeneous freezing at conditions below the homogeneous freezing threshold (DeMott et al., 1998; Heymsfield et al., 1998; Rogers et al., 1998; Seifert et al., 2003).

In heterogeneously induced cirrus the maximum supersaturation is limited to values below the homogeneous freezing threshold as the ice crystals grow by the uptake of water vapour. This results in optically thin layers of cloud comprised of a low number of large crystals which are radiatively different to their homogeneously induced counterparts (Gierens, 2003; Kärcher and Lohmann, 2003).

Given its ubiquity in the atmosphere, if soot behaves as an efficient ice nucleus (IN) then it may have potential to impact climate by modifying the lifecycle and optical properties of mixed phase and glaciated clouds (DeMott et al., 1997; Gierens, 2003; Lohmann, 2002a; Lohmann and Feichter, 2005) particularly in sensitive regions of the globe such as the Arctic and Antarctic. Soot may offer significant concentrations of active IN in the lower troposphere where an increase in ice crystal number concentration may result in more rapid and frequent glaciation of mixed phase clouds by the Bergeron-Findeisen process (Lohmann and Feichter, 2005; Rogers and Yau, 1996; Schwarzenbock et al., 2001). This would likely act to reduce cloud top albedo and increase ice phase precipitation, reducing cloud lifetime. However these effects are highly uncertain and estimates of the forcings associated with IN are largely unknown

ACPD
11, 11007–11038, 2011

(Lohmann, 2002a; Lohmann and Feichter, 2005; Penner et al., 2001). The effects of soot will be of great significance if the type of soot emitted can act as an efficient ice nucleus or if once in the atmosphere it is processed in such a way as to promote ice activation. Studies by DeMott et al. (1999) and Kärcher and Lohmann (2003) suggest that the activation of ice upon soot may explain the formation of visible contrails behind aircraft. Modelling studies by Jensen and Toon (1997) showed that cirrus formed by homogeneous freezing is markedly different in behaviour to that formed by heterogeneous freezing mechanisms: homogeneously nucleated cirrus was shown to be transient in nature, precipitating quickly whereas cirrus formed by the heterogeneous freezing on soot was found to be much more persistent and diffuse. More recently studies by Kärcher et al. (2007) concluded that the effect of aircraft soot on cirrus formation is highly complex and was dependent on many emission and environmental parameters; the use of a microphysical-chemical model found that high concentrations of soot may increase the number of ice crystals and conversely low concentrations of soot coagulated with background aerosol could significantly reduce ice crystal number. It was noted that the source and ageing processes were crucial factors in determining the ice nucleation efficiency of soot, stating that coated soot particles are poor ice nuclei when compared to their bare counterparts (Kärcher et al., 2007).

There have been relatively few laboratory studies examining soot's behaviour as a potential IN partly due to the difficulty in designing an experiment to probe the soot particles subsequently contained within cloud ice crystals and also because of the problems inherent in sourcing suitable and reproducible test soot. Investigations have used different experimental techniques and different soot production and characterisation methods which also makes direct comparison of reported results difficult, however they all suggest that soot may be a significant source of atmospheric IN as noted by Dymarska et al. (2006) (DeMott, 1990; Diehl and Mitra, 1998; Dymarska et al., 2006; Gorbunov et al., 2001; Kärcher et al., 2007; Möhler et al., 2005a,b). The development of the single particle soot photometer (SP2) has added to our ability to measure soot size and concentrations with high sensitivity, and is ideally suited for this type of

ACPD
11, 11007–11038, 2011

analysis. Analysis of the SP2 data has allowed us to examine the mixing state and coating physical properties of the produced test soot and to compare soots of different organic carbon content. Since the SP2 measures both elastic scatter and incandescence it is possible to determine whether the sample aerosol contains incandescent material, allowing the fraction of the aerosol population containing refractory black carbon to be estimated. Baumgardner et al. (2008) used an SP2 in conjunction with a PCVI and forward facing inlet onboard the National Center for Atmospheric Research Gulfstream-V aircraft to sample refractory black carbon (rBC) in and out of cloud. They were able to derive the number fraction of residuals containing black carbon and found that twice as many residuals contained black carbon particles compared to particles measured in cloud-free air (Baumgardner et al., 2008).

2 Experimental method

2.1 Cloud chamber and soot generation

Cloud simulation experiments were performed in the large Aerosol Interactions and Dynamics in the Atmosphere (AIDA) chamber facility (Benz et al., 2005; Möhler et al., 2008, 2005a, 2006). The 84 m^3 aerosol vessel (Fig. 1) is enclosed within a large insulating box that can be chilled to a temperature of 238 K using conventional compressors. Evaporating liquid nitrogen in the heat exchangers can further cool the chamber to a temperature of 183 K. The aerosol vessel is initially evacuated to a pressure below 0.1 hPa and then refilled with particle free synthetic air to minimise the background aerosol concentration (N_p <0.1 cm^{-3}). The chamber walls are coated with a thin layer of ice which maintains a high relative humidity of 90–95% with respect to ice within the vessel under constant temperature and pressure conditions. Supersaturation with respect to ice can be achieved through expansion cooling by reducing the vessel pressure with two large pumps through a 10 cm diameter pipe connected to the top of the chamber. The cooling rate can be varied between 0.1 to 4 K min^{-1}, assuming a dry

ACPD
11, 11007–11038, 2011

adiabatic lapse rate of 9.75 K km^{-1} this equates to updraft velocities of 0.15 ms^{-1} to 6.5 ms^{-1} in the troposphere, respectively (Möhler et al., 2003). Further details of the AIDA facility and its instrumentation can be found in (Möhler et al., 2008, 2005a,b, 2003; Wagner et al., 2009).

Combustion soot aerosol was generated using a Jing-CAST Technologies Combustion Aerosol Standard (CAST) propane burner. Note in this paper we use the term "soot" to refer to all particles produced by the CAST generator and "rBC" for material detected by the SP2 via laser-induced incandescence. The CAST generates the test aerosol within a co-flow diffusion of propane flame and particle free sheath air in a total flow of 29 l/min at 1013 hPa and 273 K. By varying the propane-air ratio, a range of soot containing of the order of a few percent organic carbon content to organic carbon contents of up to 80% can be generated in a repeatable fashion (Schnaiter et al., 2006). A mini-CAST (Jing-CAST Technologies) propane burner was used for a subset of experiments which may exhibit a slight change in the composition of the flame soot for the same gas flows. Soot aerosol generated by the CAST produces the majority of the number concentration in the sub-100 nm diameter range. This soot is injected into a smaller chamber (NAUA, 3.7∼ in volume) at ambient temperatures where it is left to coagulate to form a number distribution with a modal mobility diameter of approximately 300 nm as measured with a Scanning Mobility Particle Sizer before being injected into the AIDA chamber (Fig. 2). Transmission Electron Microscopy analysis showed the soot aggregates generated with the CAST to typically consist of small individual particles of aproximately 30 nm in diameter with larger spherical particles of up to 120 nm in diameter also being present (Schnaiter et al., 2006). Comparison of this soot to previous studies is difficult as in many of the studies the aerosol population was poorly defined. The Möhler et al. (2005a) study using a comercial graphite spark generator found the primary particles to be between 4 to 8 nm in diameter and these were aggregated to around 90 nm in a small chamber. Diehl and Mitra (1998) used a kerosene burner in their study to produce aggregates of 100 to 120 nm in diameter. No estimate of the primary particle size were made but it was noted by the authors

ACPD
11, 11007–11038, 2011

that 80% of the particles produced were smaller than 90 nm in diameter. DeMott et al. (1999) used comercial Degussa lamp black carbon which quotes an average size of 95 nm with aggregates being lognormally distributed with a mean diameter of 240 nm. Dymarska et al. (2006) studied a multitude of different soot types using a flow cell arrangement but only note that the majority of particles were between 1 and 20 µm in diameter. Saathoff et al. (2003) investigated soot generated using a Diesel engine which yielded primary particles smaller than 50 nm in diameter which were aggregated (along with ammonium sulphate) to modal sizes of approximately 250 nm.

For the soot characterisation experiments, three distinctly different soots were generated: (a) Minimum organic carbon content soot (~5% organic carbon content by mass), (b) Medium organic carbon content soot (~30% organic carbon content) and (c) Maximum organic carbon content soot (~60/70% organic carbon content). Hereafter these classifications for minimum, medium and maximum organic carbon content particles will be referred to as OC_5, OC_{30} and OC_{70} respectively.

During a subset of experiments the mini-CAST propane burner was used and the propane flame soot particles were coated with sulphuric acid by mixing the soot aerosol with a flow of synthetic air saturated with sulphuric acid vapour in a temperature controlled flow tube. Sulphuric acid vapour was condensed onto the soot upon cooling of the saturated mixture in a temperature gradient flow tube; the temperature in the saturator was set to 55°C and 45 °C for the OC_5 and OC_{70} experiments respectively, the temperature of the mixing region at the beginning of the coating tube was set 20 °C higher than the saturation region. Within the 1.5 m long flow tube (16 mm internal diameter) the temperature decreased to about 30 °C. The total flow rate through the coating tube was between 30 to 34 standard litres per min. The nucleation of pure sulphuric acid droplets was suppressed by adjusting the flow rates and cooling gradient profile.

2.2 Cloud, aerosol and black carbon measurements

Aerosol measurements were made by directly sampling from the AIDA chamber both prior to and during cloud simulation experiments. During cloud simulation experiments

ACPD
11, 11007–11038, 2011

it was possible to measure cloud particle residual aerosol using a Pumped Counterflow Virtual Impactor (PCVI), similar in design to that described by Boulter et al. (2006). This instrument produces a barrier flow to incoming sampled particles allowing only those greater than a certain size (i.e. with a characteristic momentum) to penetrate and be sampled. The recirculating particle-free dry barrier flow also evaporates the ice to leave the residual assumed IN, particle. Characterisation of the PCVI showed that the 50% transmission size (D_{50}) was approximately 5 µm. Aerosol residuals were analysed using a number of instruments but for this work we focus on measurements of the soot core mass and associated coating thickness made by a Single Particle Soot Photometer (SP2; DMT, Boulder, Colorado, USA, which was available for the first series of experiments examining the uncoated soot only) (Baumgardner et al., 2004; Schwarz et al., 2006; Stephens et al., 2003). Aerosol is drawn into the SP2 where the air jet containing the sample intersects a Nd:YAG, intracavity, continuous laser beam ($\lambda = 1064$ nm). Laser light scattered by sample particles of detectable size is detected by an avalanche photodetector (ADP) and related to particle size by means of calibration with polystyrene latex spheres (PSL).

Refractory and strongly light-absorbing aerosol particles (including black carbon) of sufficient size will absorb energy and become heated to their boiling or vaporization temperature when they will start to incandesce. Emitted thermal radiation is detected by narrowband (630–800 nm) and broadband (350–800 nm) filtered photo multiplier tube detectors. The signals from these are amplified to produce low and high gain signals, increasing the instruments detection resolution range. The SP2 therefore provides a measure of the total particle size distribution which can be segregated into non-absorbing (purely scattering) particles and incandescing (rBC-containing) particles. The time delay between the detection of scattering and incandescence signals from a single particle can be used as a proxy for the particle coating thickness since the coating must be ablated before the core can incandesce. The time delay is defined as the difference between the maxima in a particle's incandescence and elastic light scattering signals ($\tau_d = t_{\text{incandescence}} - t_{\text{scatter}}$) (Moteki and Kondo, 2007; Schwarz et al.,

ACPD
11, 11007–11038, 2011

2006). A detailed intercomparison study of instruments measuring the black carbon content of well characterised soot particles demonstrated that the peak incandescence signal measured by the SP2 is proportional to black carbon mass and that for a given mass the incandescence signal is independent of particle morphology or mixing state (Slowik et al., 2007).

The SP2 was aligned and tested prior to the start of the experiment series and the instrument was calibrated daily before each series of experiments using glassy carbon spheres (Alpha Aesar, density 1.42 g cm^{-3}) which were size selected using a DMA (TSI, model 3077), and polystyrene latex sphere test particles to verify the calibration and optical alignment of the instrument. As configured in this experiment, the SP2 typically detected single particles in a mass range of 7–370 fg, equivalent to particles with 190–730 nm rBC core diameters, calculated from the particle mass assuming a rBC density of 1.8 g cm^{-3} however the CAST soot (rBC plus associated material) may have densities of between 1.3 and 1.9 g cm^{-3} depending on OC content. The glassy carbon particle calibration covered a mass range 20–250 fg (270-650 nm for soot density of 1.8 g cm^{-3} (Bond and Bergstrom, 2006). The detectable size range for purely scattering particles was 150–600 nm diameter and PSL calibrations were performed over a size range from 200–600 nm. A detailed description of the data processing and analysis procedures developed for the University of Manchester SP2 is provided by Liu et al. (2010) and McMeeking et al. (2010).

Ice particle concentration and size was measured independently with an optical particle counter (OPC) and a Cloud Particle Imaging probe (CPI; SPEC, Model 1). The optical particle counter (WELAS model 2000, Palas GmbH) is sensitive to ice particles in the size range of 1–20 µm in diamater and measured the size and number concentration from a vertical sample flow tube attached directly beneath the aerosol chamber. A CPI was also mounted directly below the aerosol chamber and used to measure the concentration and size distribution of large ice crystals with diameters, D_p >10 µm, and to identify their morphology. The CPI instrument and the analysis techniques used are the same as those described by Connolly et al. (2007, 2009).

ACPD
11, 11007–11038, 2011

The ice saturation ratio (S_{ice}) was calculated from the water vapour pressure e_w that was measured in situ by a tuneable diode laser (TDL) absorption spectrometer. The instrument consists of a room temperature near-infrared tunable diode laser operating at a wavelength of (1370±2) nm and a White multipath cell with 23–99 m optical path (Ebert et al., 2005). The TDL system provides water vapour mixing ratio data with a time resolution of 1 Hz, an accuracy of ±5–10%, and a resolution in the region of 15 ppb as has been demonstrated during the international hygrometer intercomparison AquaVIT (Fahey et al., 2009). The water vapour saturation pressure with respect to ice was calculated according to the parameterisation of Murphy and Koop (2005).

3 Experimental parameters and soot characterisation

Two sets of ice cloud nucleation experiments using CAST and mini-CAST propane flame soot particles with the OC_5, OC_{30} and OC_{70} content were carried out with and without a sulphuric acid (SA) coating. Seven experiments in total were conducted without SA coatings during the campaign, referred to hereafter as IN09 (March 2006). The parameters describing the experimental conditions and aerosol loadings for all the IN09 experiments are summarised in Table 1 along with the conditions at the onset of freezing. The onset of freezing conditions are defined as those where a given fraction of the test aerosol becomes ice active. In this work activation thresholds of 0.1% and 1% were initially used however given the low aerosol number concentrations for IN09 the 0.1% activation threshold may possibly be biased by background aerosol activation and so is excluded from the final discussions. Typical background activation concentrations from reference expansions were found to be approximately 0.5 cm^{-3}. A further series of 11 experiments (referred to as the IN11 campaign, November 2007) studied the ice nucleation properties of mini-CAST propane flame soot particles with and without sulphuric acid coatings; the experimental conditions for the IN11 experiment are summarised in Table 1.

ACPD
11, 11007–11038, 2011

The OC_5 and OC_{30} flame soot were characterised both prior to cloud expansion experiments at equilibrium in the AIDA chamber and during cloud expansion experiments using a PCVI. We treat the particles as rBC "cores" associated with organic coatings when interpreting the SP2 measurements. The top left and middle left panels of Fig. 3 show the time delay, τ_d, between SP2 scattering and incandescence signals for the OC_5 and OC_{30} soot particles prior to cloud expansion as a function of the black carbon core size. The OC_5 and OC_{30} soot display significantly different time delay characteristics; the modal value of τ_d for the OC_5 soot is 0.6 µs at a BC core size (D_{BC}) of 0.25 µm. This is indicative of an undetectable coating and is similar to the time delays observed for uncoated calibration particles. In contrast the OC_{30} soot modal τ_d is 5.8 µs at $D_{BC} = 0.19$ µm. Values of $\tau_d = 4.2$ µs are considered to be indicative of particles with a thick coating (Liu et al., 2010) thus the OC_{30} soot has a considerably thicker or less volatile coating than the OC_5 soot. The BC core sizes for the OC_5 were larger and more varied than the OC_{30} soot which may be due to the bulk of the mass residing in the core consisting of a chain aggregate fractal morphology whereas the OC_{30} soot has most of its mass residing in the coating. Previous work by Schnaiter et al. (2006) showed that soot of similar organic carbon content to the OC_{30} soot generated by CAST contained spheroidal particles of sizes up to 120 nm in diameter which were presented individually or in small aggregates. Analysis of the scattering and incandescence of the pre-expansion soot found that for the OC_5 soot 1 in every 420 particles exhibited no incandescence. For the OC_{30} soot this was found to be approximately 1 in 21 particles.

The difference in τ_d between the pre-expansion and residuals for the OC_5 soot is small, $\tau_d = 0.4$ µs, $D_{BC} = 0.28$ µm ($\Delta\tau_d = -0.2$ µs, $\Delta D_{BC} = 0.03$ µm), however the BC core size mode is broader and moves to larger mean sizes suggesting either that larger soot-core particles activate preferentially or that all sizes activate with equal efficiency but that the ice produced inertially scavenges additional unactivated particles which increases the size of the residual core. Very few OC_{30} soot particles are ice active, typically 2–3% of the population, resulting in poor counting statistics for the

ACPD
11, 11007–11038, 2011

PCVI residual measurement in this case, thus no meaningful comparison between the pre-expansion and residual data can be made. Artefacts from incomplete evaporation of cloud particles in the PCVI are minimal for the OC_5 soot; if the coating thickness was increased by incomplete evaporation it would be expected that there would be a significant shift in the modal value of τ_d between the pre-expansion and residual particles. To test this several τ_d probability densities of narrow core mass range (5 fg) were compared for the pre-expansion and residual soot where no significant modal variation was observed, however, there were some outliers spreading to high τ_d in the residuals, suggesting that a minority of the residual particles have an increased coating thickness. If the PCVI were to remove volatiles from the coating then it would be expected that the modal value of τ_d would decrease which is not consistent with the observations, however the SP2 may not be sufficiently sensitive to measure such a decrease. The τ_d probability density integrated over the size range of the SP2 for the above cases is given in the bottom left panel of Fig. 3 where it can be seen that the OC_5 and OC_{30} τ_d distributions are significantly different due to the difference in coating thickness. The OC_5 τ_d distributions for the pre-expansion and residuals are similar and any differences are likely to be due to differences in the measured size distributions of each case. This is also observed in the OC_5 incandescent mass probability distribution (bottom right panel, Fig. 3) where fewer low mass particles are observed in the residuals when compared to the pre-expansion sample, again suggesting that the larger soot particles are preferentially activated. Previous studies have observed similar phenomena for dust particles; Archuleta et al. (2005) reported size dependent ice activation efficiencies for several mineral dusts where they noted that larger particles consistently nucleated ice at lower humidity than smaller particles at the same temperature. Möhler et al. (2006) also showed that larger dust particles are more ice active than smaller particles owing to their larger surface area on which nucleation can occur.

ACPD
11, 11007–11038, 2011

3.1 Influence of organic carbon content

A series of cloud simulation experiments starting at an initial temperature of 228 K and with constant pumping rates were performed using the three test soots. The left hand column of Fig. 4 shows a time series of temperature, (T), pressure, (P), supersaturation with respect to ice (S_{ice}) and water (S_{water}), ice number concentration (N_{ice}) measured with the WELAS OPC (black line) and CPI (blue line), and the percentage of the aerosol population that has become ice active for the OC_5 soot. For the OC_5 soot (experiment IN09_08) the onset of freezing occurs well below water saturation suggesting the particles are active as deposition freezing nuclei; approximately 25% of the soot particles were observed to activate during this experiment. From the time series of particle concentrations a formation rate of $\sim 1.20\,cm^{-3}\,s^{-1}$ was subsequently calculated over the period from the initiation of the ice phase to the maximum observed ice number. At the onset of freezing the ratio of rBC to purely scattering particles detected by the SP2 in the residual aerosol was approximately 7, indicating that the ice active aerosol largely contains incandescent material, thus the OC_5 soot is ice active. A subsequent expansion on the same test soot under similar conditions (IN09_09) yielded a similar onset of freezing for the 1% ice activation threshold within experimental error. When compared to the onset of freezing for pure sulphuric acid solution droplets Möhler et al. (2003) it can be seen that the OC_5 flame soot acts as a deposition nucleus at much lower S_{ice} than is required for homogeneous freezing of solution droplets at the same temperature.

The OC_{30} flame soot (experiment IN09_18, Fig. 4, middle column) displays somewhat different nucleation characteristics to the OC_5 soot. The 1% ice active onset of freezing occurs above water saturation with a significantly lower ice particle formation rate of $\sim 0.05\,cm^{-3}\ s^{-1}$ with only 1% of the aerosol being ice active. The ratio of incandescent particles to scattering particles in the residuals also is low (20–60%) although the counting statistics are limited. Subsequent expansions on the same test soot (IN09_19 and IN09_20) yielded a similar onset of freezing for the 1% ice activation

ACPD
11, 11007–11038, 2011

threshold within experimental error.

The right hand column of Fig. 4 shows the time series of the OC_{70} soot experiment (IN09_21). Similar to the OC_{30} experiment, the onset of freezing occurs near water saturation, however, the formation rate is significantly higher at ~0.19 $cm^{-3}\,s^{-1}$. In this case 3–5% of the aerosol became activated. The majority of residual particles do not incandesce and only small cores are observed with low refractory BC mass fraction. Similar to previous experiments, subsequent expansion experiments on the same soot did not yield significant differences in the onset of freezing.

The above experiments on the uncoated soot are summarised in Fig. 5 where the onset of freezing is shown as a function of temperature and ice saturation ratio. It can clearly be seen that the OC_5 soot became ice active as deposition nuclei below water saturated conditions whereas the OC_{30} and OC_{70} soots required water saturation for ice nucleation to occur.

3.2 Influence of sulphuric acid coating

The second series of experiments (IN11) examined how the ice nucleating behaviour of mini-CAST propane soot particles was altered by the addition of a sulphuric acid coating. It was found that the addition of the coating acted to shift the freezing threshold of OC_5 soot to higher ice saturation ratios than were necessary for the uncoated soot to become ice active as is shown in Fig. 7. The uncoated OC_5 flame soot activated to form ice below water saturation by deposition nucleation in a similar fashion to the previous series of experiments. When a sulphuric acid coating was applied the onset of freezing for 0.1% of the aerosol population (IN11_24, Fig. 7) occured at conditions typical of the homogeneous freezing sulphuric acid as characterised by Koop et al. (2000). The time series of ice crystal number concentration for the OC_5 soot with sulphuric acid coating is shown in the left column of Fig. 6 where it can be seen that there is a sharp increase in ice crystal number concentration as measured by the WELAS shortly after the onset of freezing. The RH at the onset of freezing along with the ice formation rate (2.18 $cm^{-3}\,s^{-1}$) indicates that ice is mainly formed by the homogeneous freezing

ACPD
11, 11007–11038, 2011

of sulphuric acid mixed with organics from the flame soot. However, a contribution from immersion freezing cannot be ruled out.

The OC_{30} mini-CAST soot was found to be inactive when uncoated. Ice activation behaviour was not observed until S_i values of 2.2–2.38 (T_g = 219.4–218.6 K, S_w in excess of 1.3) was achieved, considerably higher than the results reported for IN09 using the CAST burner. The reason for this is unclear; possible explanations are that the generated soot is extremely hydrophobic or that the organic coating has undergone a glassy transition resulting in ice crystal growth being significantly impeded which has recently been independently demonstrated by Zobrist et al. (2008) and Murray (2008). When the OC_{30} soot is coated with sulphuric acid the onset of freezing occurs slightly above the homogeneous freezing threshold for sulphuric acid suggesting that similar to the OC_5 case, the homogeneous freezing of the mixed coating is the dominant process.

The uncoated OC_{70} mini-CAST soot became ice active at water saturation similar to the OC_{70} CAST soot. Subsequent expansions on the same soot showed that significant IN activity required water saturation. The addition of a sulphuric acid coating required conditions for the onset of freezing that were similar to those for homogeneous freezing of sulphuric acid, again suggesting homogeneous freezing to be the dominant mode. The results of the above experiments are summarised in Fig. 7 where the onset of freezing is shown as a function of temperature and ice saturation ratio. The mean conditions at the onset of freezing are given in Table 2. The addition of a sulphuric acid coating acts to impede the ease with which the OC_5 flame soot will become ice active when comparing IN11_20 to IN11_24, however for the second consecutive expansion on the test soot (IN11_22 and IN11_25) little change was observed. The addition of a sulphuric acid coating to the OC_{30} and OC_{70} mini-CAST soots resulted in a significant reduction in the threshold of the onset of freezing, making them more active IN.

ACPD
11, 11007–11038, 2011

4 Summary and conclusions

The critical saturation ratios for the onset of freezing of propane flame soot particles with and without sulphuric acid coatings as a function of organic carbon content were investigated. Ice initiation was achieved in cloud simulation expansion experiments with cooling rates between −0.7 to −2.1 K min^{-1}. For uncoated soot, ice nucleation occured at a minimum threshold of S_{ice} ~1.22 at T = 226.6 K for the OC_5 test soot by deposition freezing. The OC_{30} case required supersaturation with respect to water for ice formation to occur as did the OC_{70} flame soot case. This suggests that either the higher OC flame soots activate by condensation freezing or only act as freezing nuclei after liquid droplet activation, which is in agreement with previous studies by DeMott (1990) using flame soot particles. It is suggested that the variation in ice activation threshold may be due to the different soot core sizes with larger cores exhibiting lower thresholds.

The addition of a sulphuric acid coating was observed to alter the ice nucleation threshold for all of the test soot. For the OC_5 soot the coating acted to increase the activation threshold for the initial expansion, effectively making it a less active ice nucleus. This is in agreement with Möhler et al. (2005a). For the subsequent expansion on the coated OC_5 soot the coating acted to slightly decrease the activation threshold when compared to the subsequent expansion on the uncoated soot. The mechanism for this is unclear.

The addition of sulphuric acid coatings to the OC_{30} and OC_{70} soots acted to significantly reduce the threshold required for ice activation as the particles undergo homogeneous freezing. This is in agreement with the work of DeMott et al. (1999), who showed that addition of multiple layers of H_2SO_4 to Degussa soot would reduce the RH_w required for ice nucleation by as much as 10%. This is contrary however to the result of Möhler et al. (2005a) who showed that spark generator soot became less efficient IN when coated with sulphuric acid. However, a key point here is that the uncoated spark generator soot was shown to be a highly efficient IN, which is not true of the OC_{30}

ACPD
11, 11007–11038, 2011

and OC_{70} flame soot used here. The Möhler et al. (2005a) study notes that there is a discrepancy between their findings and the DeMott et al. (1999) study and states that there may be a relationship between the ice nucleation efficiency of the soot and how it behaves when coated with sulphuric acid. This result demonstrates that it is important to know the organic carbon content of soot and its mixing state with sulphuric acid in order to fully assess its impact as an ice nucleus and further investigation is clearly required.

It has been shown that propane flame soot acts as an efficient deposition mode IN if it has a sufficiently low organic carbon content and is uncoated. Should the soot be similar to those types found in aircraft exhaust emissions then they may be significant for so-called soot-induced cirrus as described by Jensen and Toon (1997) and Kärcher et al. (2007), where the exhaust soot disperses to form or modify cirrus cloud. Modelling studies by Kärcher (2004) showed that heterogeneous freezing can significantly dehydrate the tropical tropopause if the IN present freeze at low supersaturations ($RH_i = 130$) or are at least present in abundance ($N_p \geq 10\ L^{-1}$). The minimum organic carbon content soot satisfies these criteria, allowing this soot to potentially alter the moisture budget in this region significantly (Kärcher, 2004). However, it is important to know the mixing state as coatings may act to reduce soot ice activity the conditions specified by the Kärcher study. Studies in the upper troposphere and lower stratosphere by Schwarz et al. using an SP2 found that 60–80% of the black carbon was internally mixed with other material (Schwarz et al., 2008). Liu et al. (2010) reported that 40±15% of observed BC particles in the free troposphere over Switzerland were mixed with large amounts of non-refractory materials present as a thick coating surrounding the BC core. Given the findings of this paper, such coatings would act to reduce the efficiency of OC_5 soot as an ice nuclei such that they may not activate at RH_i ≤130, however this poor IN behaviour may be compensated for if they exceed concentrations ≥10 L^{-1}.

ACPD
11, 11007–11038, 2011

Acknowledgements. This work was funded by the NERC APPRAISE programme, grant number NE/E01125X/1. Part of the AIDA work was funded within the European Union Integrated Project SCOUT-O3. Technical support by the AIDA team is gratefully acknowledged. Instrumentation and instrument scientist support provided by NERC National Centre for Atmospehricv Science (NCAS) and the NCAS Facility for Ground Based Measurements (FGAM). I. Crawford was supported by a NERC studentship NER/S/A/2004/12355.

References

Archuleta, C. M., DeMott, P. J., and Kreidenweis, S. M.: Ice nucleation by surrogates for atmospheric mineral dust and mineral dust/sulfate particles at cirrus temperatures, Atmos. Chem. Phys., 5, 2617–2634, doi:10.5194/acp-5-2617-2005, 2005. 11009, 11018

Baumgardner, D., Kok, G., and Raga, G.: Warming of the Arctic lower stratosphere by light absorbing particles, Geophys. Res. Lett., 31, L06117, doi:10.1029/2003GL018883, 2004. 11014

Baumgardner, D., Subramanian, R., Twohy, C., Stith, J., and Kok, G.: Scavenging of black carbon by ice crystals over the northern Pacific, Geophys. Res. Lett., 35, D04204, doi:10.1029/2005JD006627, 2008. 11011

Benz, S., Megahed, K., Möhler, O., Saathoff, H., Wagner, R., and Schurath, U.: T-dependent rate measurements of homogeneous ice nucleation in cloud droplets using a large atmospheric simulation chamber, J. Photochem. Photobiol. A: Chemistry, 176, 208–217, 2005. 11011

Bond, T. and Bergstrom, R.: Light Absorption by Carbonaceous Particles: An Investigative Review, Aerosol Sci. Technol., 40, 27–67, doi:10.1080/02786820500421521, 2006. 11015

Boulter, J., Cziczo, D., Middlebrook, A., Thomson, D., and Murphy, D.: Design and Performance of a Pumped Counterflow Virtual Impactor, Aerosol Sci. Technol., 40, 969–976, 2006. 11014

Connolly, P. J., Flynn, M. J., Ulanowski, Z., Choularton, T. W., Gallagher, M. W., and Bower, K. N.: Calibration of the Cloud Particle Imager Probes Using Calibration Beads and Ice Crystal Analogs: The Depth of Field, J. Atmos. Ocean. Technol., 24, 1860–1879, 2007. 11015

Connolly, P. J., Möhler, O., Field, P. R., Saathoff, H., Burgess, R., Choularton, T., and Gallagher,

ACPD

11, 11007–11038, 2011

M.: Studies of heterogeneous freezing by three different desert dust samples, Atmos. Chem. Phys., 9, 2805–2824, doi:10.5194/acp-9-2805-2009, 2009. 11015
DeMott, P.: An Exploratory Study of Ice Nucleation by Soot Aerosols, J. Appl. Meteorol., 29, 1072–1079, 1990. 11010, 11022
DeMott, P. J., Rogers, D. C., and Kreidenweis, S. M.: The susceptibility of ice formation in upper tropospheric clouds to insoluble aerosol components, J. Geophys. Res. Atmos., 102, 19575–19584, 1997. 11009
DeMott, P. J., Rogers, D. C., Kreidenweis, S. M., Chen, Y., Twohy, C. H., Baumgardner, D., Heymsfield, A. J., and Chan, K. R.: The role of heterogeneous freezing nucleation in upper tropospheric clouds: Inferences from SUCCESS, Geophys. Res. Lett., 25, 1387, doi:10.1029/97GL03779, 1998. 11009
DeMott, P., Chen, Y., Kreidenweis, S., Rogers, D., and Sherman, D.: Ice formation by black carbon particles, J. Geophys. Res. Lett., 26, 2429–2432, 1999. 11010, 11013, 11022, 11023
Diehl, K. and Mitra, S. K.: A laboratory study of the effects of a kerosene-burner exhaust on ice nucleation and the evaporation rate of ice crystals, Atmos. Environ., 32, 3145–3151, 1998. 11010, 11012
Dymarska, M., Murray, B., Sun, L., Eastwood, M., Knopf, D., and Bertram, A.: Deposition ice nucleation on soot at temperatures relevant for the lower troposphere, J. Geophys. Res., 111, D04204, doi:10.1029/2005JD006627, 2006. 11010, 11013
Ebert, V., Teichert, H., Giesemann, C., Saathoff, H., and Schurath, U.: Fiber-coupled in-situ laser absorption spectrometer for the selective detection of water vapour traces down to the ppb-level, Tech. Mess., 72, 23–30, 2005. 11016
Fahey, D., Gao, R. S., and Moehler, O.: Summary of the AquaVIT Water Vapour Intercomparison: Static Experiments, available online at: https://aquavit.icg.kfa-juelich.de/AquaVit/AquaVitWiki, 2009. 11016
Field, P., Cotton, R. J., Johnson, D., Noone, K., Glantz, P., Kaye, P. H., Hirst, E., Greenaway, R. S., Jost, C., Gabriel, R., Reiner, T., Andreae, M., Saunders, C. P. R., Archer, A., Choularton, T., Smith, M., Brooks, B., Hoell, C., Bandy, B., and Heymsfield, A.: Ice nucleation in orographic wave clouds: Measurements made during INTACC, Q. J. Roy. Meteorol. Soc., 127, 1493–1512, 2001. 11009
Gierens, K.: On the transition between heterogeneous and homogeneous freezing, Atmospheric chemistry and physics, 3, 437–446, 2003. 11009
Gorbunov, B., Baklanov, A., Kakutkina, N., Windsor, H. L., and Toumi, R.: Ice nucleation on

ACPD
11, 11007–11038, 2011

soot particles, Journal of aerosol science, 32, 199–215, 2001. 11010
Haag, W., Karcher, B., Strom, J., Minikin, A., Lohmann, U., Ovarlez, J., and Stohl, A.: Freezing thresholds and cirrus cloud formation mechanisms inferred from in situ measurements of relative humidity, Atmos. Chem. Phys., 3, 1791–1806, doi:10.5194/acp-3-1791-2003, 2003. 11009
Heymsfield, A. J. and Miloshevich, L. M.: Homogeneous Ice Nucleation and Supercooled Liquid Water in Orographic Wave Clouds, J. Atmos. Sci., 50, 2335–2353, 1993. 11009
Heymsfield, A. J. and Sabin, R. M.: Cirrus Crystal Nucleation by Homogeneous Freezing of Solution Droplets, J. Atmos. Sci., 46, 2252–2264, 1989. 11009
Heymsfield, A. J., Miloshevich, L. M., Twohy, C., Sachse, G., and Oltmans, S.: Upper-tropospheric relative humidity observations and implications for cirrus ice nucleation, Geophys. Res. Lett., 25, 1343, doi:10.1029/98GL01089, 1998. 11009
Jensen, E. and Toon, O.: The potential impact of soot particles from aircraft exhaust on cirrus clouds, Geophys. Res. Lett., 24, 249–252, 1997. 11010, 11023
Jensen, E. J., Toon, O. B., Tabazadeh, A., Sachse, G. W., Anderson, B. E., Chan, K. R., Twohy, C. W., Gandrud, B., Aulenbach, S. M., Heymsfield, A., Hallett, J., and Gary, B.: Ice nucleation processes in upper tropospheric wave-clouds observed during SUCCESS, Geophys. Res. Lett., 25, 1363, doi:10.1029/98GL00299, 1998. 11009
Kärcher, B.: A Parameterization of cirrus cloud formation: Homogeneous freezing including effects of aerosol size, J. Geophys. Res., 107, 4698, doi:10.1029/2001JD001429, 2002. 11009
Kärcher, B.: Cirrus clouds in the tropical tropopause layer: Role of heterogeneous ice nuclei, Geophys. Res. Lett., 31(1–5), L12101, doi:10.1029/2004GL019774, 2004. 11023
Kärcher, B. and Lohmann, U.: A parameterization of cirrus cloud formation: Heterogeneous freezing, J. Geophys. Res., 108, 4402, doi:10.1029/2002JD003220, 2003. 11009, 11010
Kärcher, B., Moehler, O., DeMott, P. J., Pechtl, S., and Yu, F.: Insights into the role of soot aerosols in cirrus cloud formation, Atmos. Chem. Phys., 7, 4203–4227, doi:10.5194/acp-7-4203-2007, 2007. 11010, 11023
Koop, T., Luo, B. P., Tsias, A., and Peter, T.: Water activity as the determinant for homogeneous ice nucleation in aqueous solutions, Nature, 406, 611–614, 2000. 11009, 11020, 11036, 11038
Liu, D., Flynn, M., Gysel, M., Targino, A., Crawford, I., Bower, K., Choularton, T., Jurányi, Z., Steinbacher, M., Hüglin, C., Curtius, J., Kampus, M., Petzold, A., Weingartner, E., Bal-

ACPD
11, 11007–11038, 2011

tensperger, U., and Coe, H.: Single particle characterization of black carbon aerosols at a tropospheric alpine site in Switzerland, Atmos. Chem. Phys., 10, 7389–7407, doi:10.5194/acp-10-7389-2010, 2010. 11015, 11017, 11023
Lohmann, U.: A glaciation indirect aerosol effect caused by soot aerosols, Geophys. Res. Lett., 29, 1052, doi:10.1029/2001GL014357, 2002a. 11009, 11010
Lohmann, U.: First interactive simulations of cirrus clouds formed by homogeneous freezing in the ECHAM general circulation model, J. Geophys. Res. Atmos., 107(D10), 4105, doi:10.1029/2001JD000767, 2002b. 11009
Lohmann, U. and Feichter, J.: Global indirect aerosol effects: a review, Atmos. Chem. Phys., 5, 715–737, doi:10.5194/acp-5-715-2005, 2005. 11009, 11010
Marti, J. and Mauersberger, K.: A survey and new measurements of ice vapour pressure at temperatures between 170 and 250 K, Geophys. Res. Lett., 5, 363–366, 1993. 11009
McMeeking, G. R., Hamburger, T., Liu, D., Flynn, M., Morgan, W. T., Northway, M., Highwood, E. J., Krejci, R., Allan, J. D., Minikin, A., and Coe, H.: Black carbon measurements in the boundary layer over western and northern Europe, Atmos. Chem. Phys., 10, 9393–9414, doi:10.5194/acp-10-9393-2010, 2010. 11015
Möhler, O., Stetzer, O., Schaefers, S., Linke, C., Schnaiter, M., Tiede, R., Saathoff, H., Krmer, M., Mangold, A., Budz, P., Zink, P., Schreiner, J., Mauersberger, K., Haag, W., Kärcher, B., and Schurath, U.: Experimental investigation of homogeneous freezing of sulphuric acid particles in the aerosol chamber AIDA, Atmos. Chem. Phys., 3, 211–223, doi:10.5194/acp-3-211-2003, 2003. 11012, 11019, 11036, 11038
Möhler, O., Büttner, S., Linke, C., Schnaiter, M., Saathoff, M., Stetzer, O., Wagner, R., Kramer, M., Mangold, A., Ebert, V., and Schurath, U.: Effect of sulfuric acid coating on heterogeneous ice nucleation by soot aerosol particles, J. Geophys. Res., 110, D11210, doi:10.1029/2004JD005169, 2005a. 11010, 11011, 11012, 11022, 11023
Möhler, O., Linke, C., Saathoff, H., Schnaiter, M., Wagner, R., Mangold, A., Krämer, M., and Schurath, U.: Ice nucleation on flame soot aerosol of different organic carbon content, Meteorologische Zeitschrift, 14, 477–484, doi:10.1127/0941-2948/2005/0055, 2005b. 11010, 11012
Möhler, O., Field, P. R., Connolly, P., Benz, S., Saathoff, H., Schnaiter, M., Wagner, R., Cotton, R., Krämer, M., Mangold, A., and Heymsfield, A. J.: Efficiency of the deposition mode ice nucleation on mineral dust particles, Atmos. Chem. Phys., 6, 3007–3021, doi:10.5194/acp-6-3007-2006, 2006. 11011, 11018

ACPD
11, 11007–11038, 2011

Möhler, O., Benz, S., Saathoff, H., Schnaiter, M., Wagner, R., Schneider, J., Walter, S., Ebert, V., and Wagner, S.: The effect of organic coating on the heterogeneous ice nucleation efficiency of mineral dust aerosols, Environ. Res. Lett., 3, 025007, doi:10.1088/1748-9326/3/2/025007 , 2008. 11011, 11012

Moteki, N. and Kondo, Y.: Effects of Mixing State on Black Carbon Measurements by Laser-Induced Incandescence, Aerosol Sci. Technol., 41, 398–417, 2007. 11014

Murphy, D. M. and Koop, T.: Review of the vapour pressures of ice and supercooled water for atmospheric applications, Q. J. Roy. Meteorol. Soc., 131, 1539–1565, doi:10.1256/qj.04.94, 2005. 11016, 11036, 11038

Murray, B. J.: Inhibition of ice crystallisation in highly viscous aqueous organic acid droplets, Atmos. Chem. Phys., 8, 5423–5433, doi:10.5194/acp-8-5423-2008, 2008. 11021

Penner, J., Andreae, M., Annegarn, H., Barrie, L., Feichter, J., Hegg, D., Jayaraman, A., Leaitch, R., Murphy, D., Nganga, J., and Pitari, G.: Climate Change 2001: The Scientific Basis: Chapter 6 Radiative Forcing of Climate Change, 2001. 11010

Rogers, D. C., DeMott, P. J., Kreidenweis, S. M., and Chen, Y.: Measurements of ice nucleating aerosols during SUCCESS, Geophys. Res. Lett., 25, 1383, doi:10.1029/97GL03478, 1998. 11009

Rogers, R. and Yau, M.: A short course in cloud physics, Oxford : Butterworth Heinemann, 3rd edn., 1996. 11009

Saathoff, H., Moehler, O., Schurath, U., Kamm, S., Dippel, B., and Mihelcic, D.: The AIDA soot aerosol characterisation campaign 1999, Journal of aerosol science, 34(10), 1277–1296, 2003. 11013

Sassen, K. and Dodd, G. C.: Homogeneous Nucleation Rate for Highly Supercooled Cirrus Cloud Droplets, J. Atmos. Sci., 45, 1357–1369, 1988. 11009

Schnaiter, M., Gimmler, M., Llamas, I., Linke, C., Jger, C., and Mutschke, H.: Strong spectral dependence of light absorption by organic carbon particles formed by propane combustion, Atmos. Chem. Phys., 6, 2981–2990, doi:10.5194/acp-6-2981-2006, 2006. 11012, 11017

Schwarz, J. P., Gao, R. S., Fahey, D. W., Thomson, D. S., Watts, L. A., Wilson, J. C., Reeves, J. M., Darbeheshti, M., Baumgardner, D. G., Kok, G. L., Chung, S. H., Schulz, M., Hendricks, J., Lauer, A., Karcher, B., Slowik, J. G., Rosenlof, K. H., Thompson, T. L., Langford, A. O., Loewenstein, M., and Aikin, K. C.: Single-particle measurements of midlatitude black carbon and light-scattering aerosols from the boundary layer to the lower stratosphere, J. Geophys. Res. Atmos., 111, D16207, doi:10.1029/2006JD007076, 2006. 11014

ACPD

11, 11007–11038, 2011

Schwarz, J. P., Spackman, J. R., Fahey, D. W., Gao, R. S., Lohmann, U., Stier, P., Watts, L. A., Thomson, D. S., Lack, D. A., Pfister, L., Mahoney, M. J., Baumgardner, D., Wilson, J. C., and Reeves, J. M.: Coatings and their enhancement of black carbon light absorption in the tropical atmosphere, J. Geophys. Res., 113, D03203, doi:10.1029/2007JD009042, 2008. 11023

Schwarzenbock, A., Mertes, S., Heintzenberg, J., Wobrock, W., and Laj, P.: Impact of the Bergeron-Findeisen process on the release of aerosol particles during the evolution of cloud ice, Atmos. Res., 58, 295–313, 2001. 11009

Seifert, M., Ström, J., Krejci, R., Minikin, A., Petzold, A., Gayet, J.-F., Schumann, U., and Ovarlez, J.: In-situ observations of aerosol particles remaining from evaporated cirrus crystals: Comparing clean and polluted air masses, Atmos. Chem. Phys., 3, 1037–1049, doi:10.5194/acp-3-1037-2003, 2003. 11009

Slowik, J. G., Cross, E. S., Han, J.-H., Davidovits, P., Onasch, T. B., Jayne, J. T., Williams, L. R., Canagaratna, M. R., Worsnop, D. R., Chakrabarty, R. K., Moosmüller, H., Arnott, W. P., Schwarz, J. P., Gao, R.-S., Fahey, D. W., Kok, G. L., and Petzold, A.: An Inter-Comparison of Instruments Measuring Black Carbon Content of Soot Particles, Aerosol Sci. Technol., 41, 295–314, 2007. 11015

Stephens, M., Turner, N., and Sandberg, J.: Particle identification by laser-induced incandescence in a solid-state laser cavity, Appl. Optics, 42, 3726–3736, 2003. 11014

Tabazadeh, A., Toon, O. B., Clegg, S. L., and Hamill, P.: A New Parameterization of H2SO4/H2O Aerosol Composition: Atmospheric Implications, Geophys. Res. Lett., 24(15), 1931–1934, 1997. 11009

Wagner, R., Linke, C., Naumann, K.-H., Schnaiter, M., Vragel, M., Gangl, M., and Horvath, H.: A review of optical measurements at the aerosol and cloud chamber AIDA, J. Quant. Spectrosc. Radiat, T., 110, 930–949, 2009. 11012

Zobrist, B., Marcolli, C., Pedernera, D. A., and Koop, T.: Do atmospheric aerosols form glasses?, Atmos. Chem. Phys., 8, 5221–5244, doi:10.5194/acp-8-5221-2008, 2008. 11021

ACPD
11, 11007–11038, 2011

Table 1. Parameters of AIDA ice cloud simulations. IN09 experiments were performed using CAST propane flame soot. P_0 is the AIDA pressure before pumping, T_{g0} the AIDA gas temperature before pumping, N_{a0} the AIDA aerosol number concentration before pumping. The onset of freezing for 0.1% and 1% of the aerosol population becoming ice active is given as a function of the AIDA gas temperature (T_g) and the saturation ratio with respect to ice and water (S_i and S_w).

Experiment parameters					0.1% activation			1% activation		
Experiment	Type	P_0, hPa	T_{g0}, K	N_{a0}, cm^{-3}	T_g, k	S_i	S_w	T_g, k	S_i	S_w
IN09_08	OC_5	989.9	228.9	210	227.3	1.10	0.71	226.6	1.22	0.78
IN09_09	OC_5	989.6	228.9	131	227.5	1.09	0.71	226.4	1.23	0.79
IN09_18	OC_{30}	996.5	228.9	277	226.9	1.21	0.79	223.6	1.63	1.02
IN09_19	OC_{30}	999.7	229.1	195	227.7	1.09	0.69	223.7	1.64	1.03
IN09_20	OC_{30}	995.0	228.9	132	227.7	1.07	0.69	223.2	1.70	1.06
IN09_21	OC_{70}	997.9	228.9	290	224.5	1.48	0.93	224.0	1.54	0.96
IN09_22	OC_{70}	990.8	228.7	180	224.3	1.52	0.95	223.9	1.67	0.99

ACPD
11, 11007–11038, 2011

Table 2. Same as Table 1 but using mini-CAST propane flame soot. Values in italics are extrapolated from the 0.1% activation data.

Experiment Parameters					0.1% activation			1% activation		
Experiment	Type	P_0, hPa	T_{g0}, K	N_{a0}, cm^{-3}	T_g, k	S_i	S_w	T_g, k	S_i	S_w
IN11_20	OC_5	997.1	228.8	1100	225.1	1.32	0.84	224.8	1.36	0.86
IN11_21	C_5	995.2	228.8	775	224.8	1.38	0.87	224.4	1.43	0.90
IN11_22	OC_5	995.3	228.8	570	224.5	1.42	0.89	224.2	1.47	0.92
IN11_24	OC_5 w/SA	999.1	228.8	1500	224.0	1.47	0.92	*223.9*	*1.48*	*0.93*
IN11_25	OC_5 w/SA	1000.2	228.8	1090	224.9	1.38	0.87	–	–	–
IN11_26	OC_{70}	1013.1	228.5	1170	222.2	>1.6	>1.0	–	–	–
IN11_27	OC_{70}	1013.0	228.3	780	220.2	>2.2	>1.3	–	–	–
IN11_28	OC_{70}	1013.2	228.3	525	218.5	2.48	1.50	–	–	–
IN11_30	OC_{70} w/SA	1015.1	228.1	1380	223.4	1.47	0.92	223.2	1.48	0.92
IN11_31	OC_{70} w/SA	1015.1	228.1	950	223.5	1.47	0.92	223.1	1.52	0.94
IN11_32	OC_{70} w/SA	1015.2	228.1	610	223.3	1.49	0.93	223.1	1.51	0.94
IN11_34	OC_{30} w/SA	1010.7	228.0	1210	223.1	1.51	0.94	*222.7*	*1.56*	*0.97*
IN11_35	OC_{30} w/SA	1007.3	228.0	860	223.1	1.53	0.95	222.9	1.56	0.97
IN11_37	OC_{30}	1002.0	228.2	1360	219.4	>2.2	>1.3	–	–	–
IN11_38	OC_{30}	1000.4	228.0	930	219.2	2.3	1.38	–	–	–
IN11_39	OC_{30}	1002.2	228.1	620	218.6	2.38	1.43	–	–	–

ACPD
11, 11007–11038, 2011

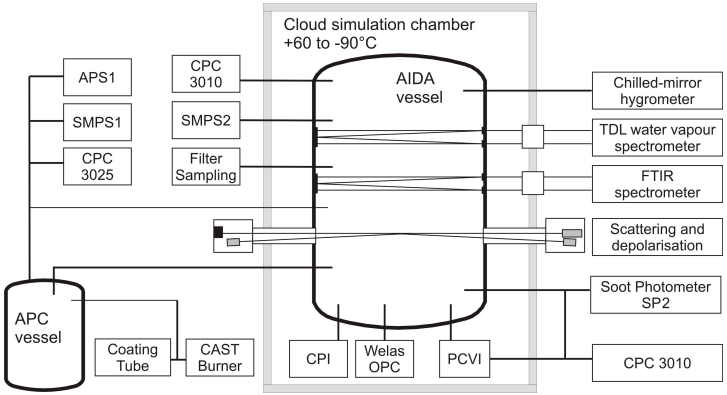

Fig. 1. Schematic of the AIDA cloud simulation chamber with instrumentation for heterogeneous ice nucleation studies of soot aerosols.

ACPD
11, 11007–11038, 2011

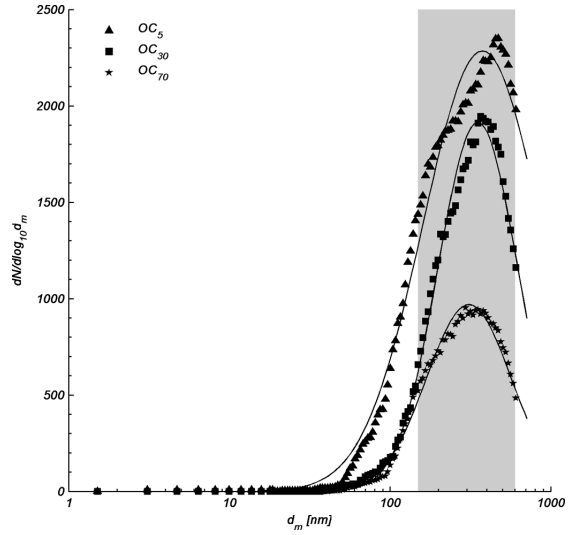

Fig. 2. Size distributions of CAST soot as measured with an SMPS; 5% (triangle), 30% (square) and 70% (star) organic carbon (OC) content after growth in the NAUA aerosol chamber prior to injection into the AIDA aerosol chamber. Area enclosed in grey shows the detection range of the SP2.

ACPD
11, 11007–11038, 2011

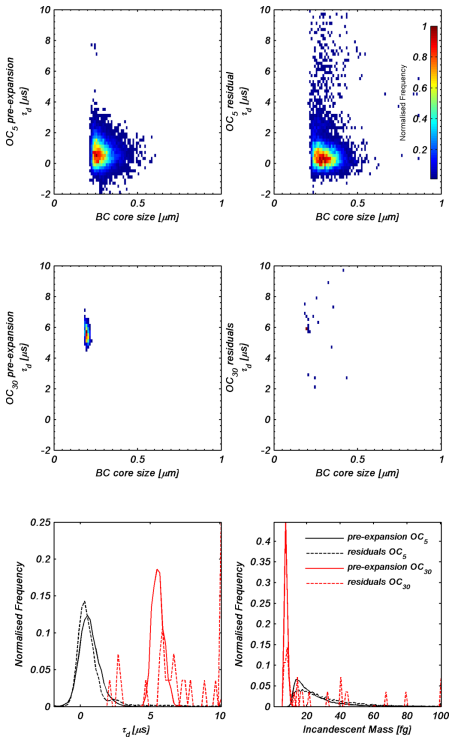

Fig. 3. Characterisation of Soot Core Size and Coating Thickness of the OC_5 and OC_{30} flame soot. Top panels display the normailized frequency of soot as a function of BC core diameter and τ_d for the OC_5 soot sampled at equilibrium in the AIDA chamber prior to a cloud expansion (left) and cloud particle residuals sampled during a cloud expansion using a PCVI (right). The frequency is normailized to the maximum observed frequency in the averaged sample. Middle panels display the same for the OC_{30} soot. Bottom panels display the τ_d probability density (left) and incandescent mass probability density (right) at all BC score sizes for the OC_5 and OC_{30} soot sampled pre-expansion at equilibrium and from PCVI residuals. The frequency of τ_d and incandescent mass are normalized by sample duration.

ACPD
11, 11007–11038, 2011

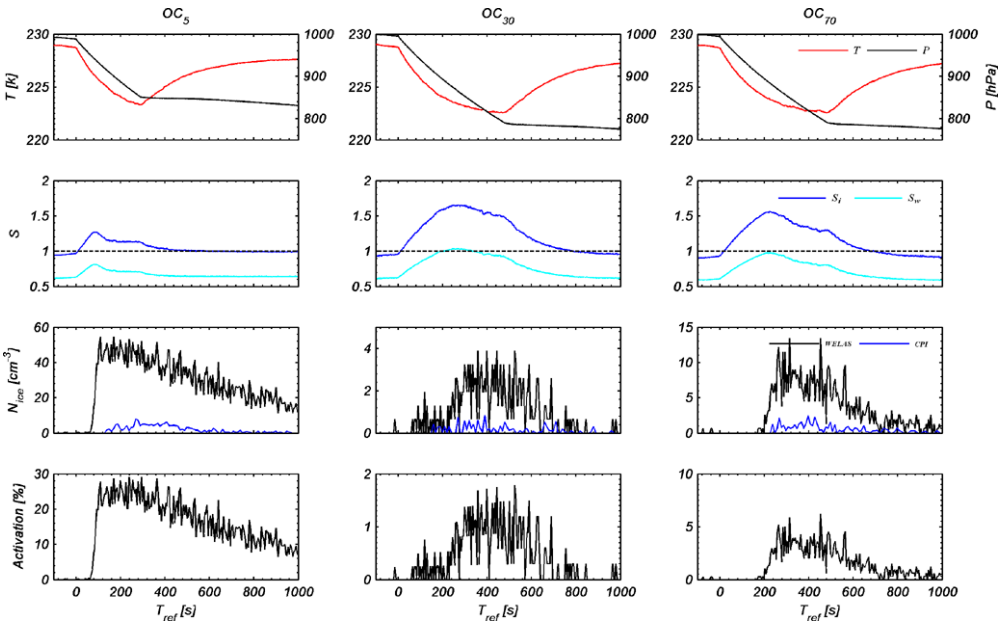

Fig. 4. Time series of temperature (T), pressure (P), saturation ratio with respect to ice and water (S), ice crystal number concentration (N_{ice}) and percentage of the aerosol population active in the ice phase for the OC_5, OC_{30} and OC_{70} flame soot.

ACPD
11, 11007–11038, 2011

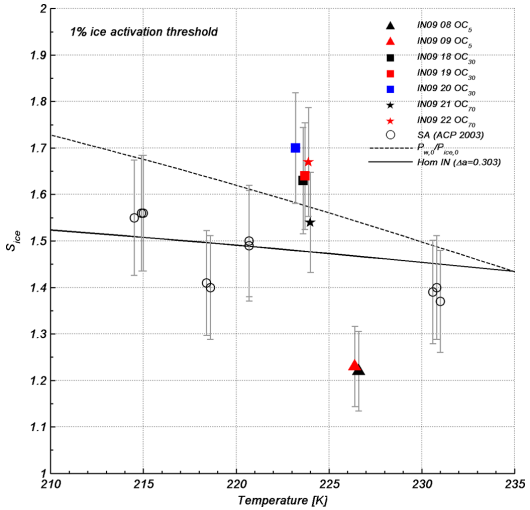

Fig. 5. Summary of T and S_{ice} for the onset of freezing for the OC_5, OC_{30} and OC_{70} flame soot particles during IN09 experiments. The dashed line indicates water saturation as given by Murphy and Koop (2005). For comparison the homogeneous freezing of pure sulphuric acid droplets are shown (ACP 2003) from previous AIDA studies Möhler et al. (2003) along with the homogeneous freezing threshold, (Hom IN) of supercooled solution droplets Koop et al. (2000), indicated by the solid line, where Δa is the fitting parameter used as described in Möhler et al. (2003) to calculate the homogeneous freezing threshold.

ACPD
11, 11007–11038, 2011

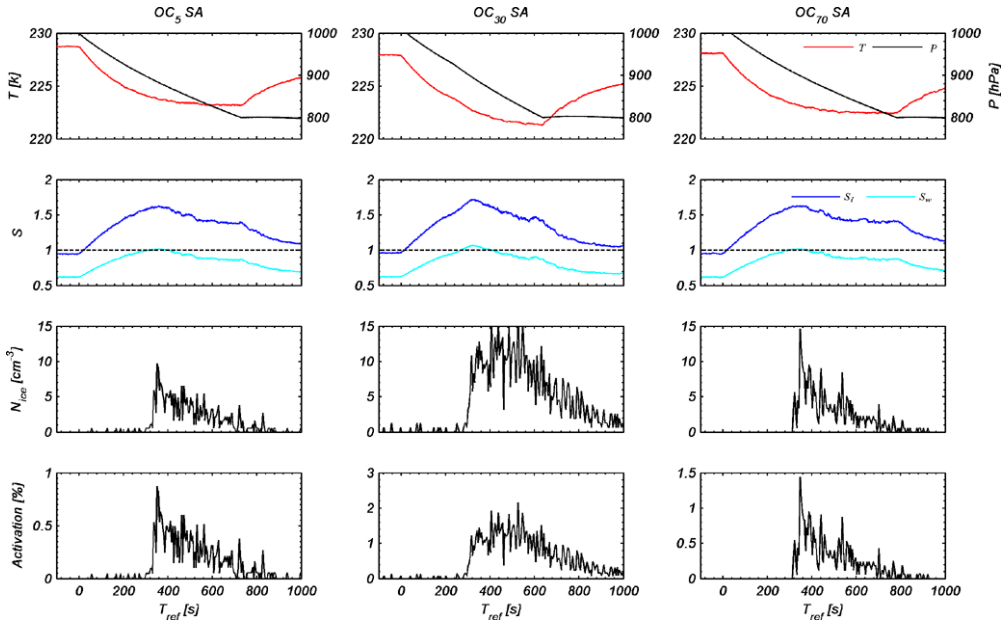

Fig. 6. same as figure 4 but for OC_5, OC_{30} and OC_{70} flame soot with sulphuric acid coating.

ACPD
11, 11007–11038, 2011

Heterogeneous freezing on propane flame soot

I. Crawford et al.

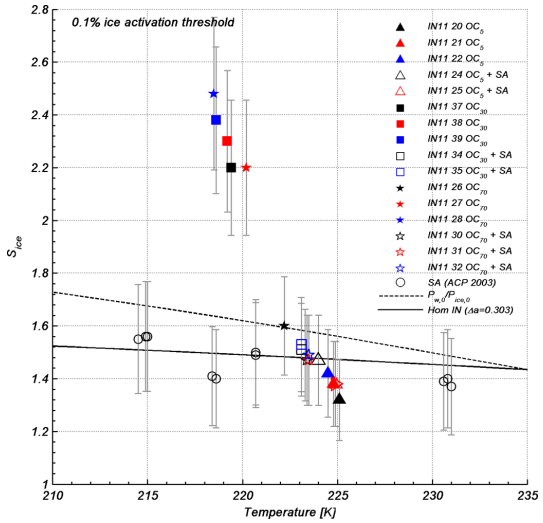

Fig. 7. Onset of freezing where 0.1% of the aerosol population become ice active for OC_5, OC_{30} and OC_{70} flame soot with (unfilled markers) and without (filled markers) a sulphuric acid coating. Dashed line is water saturation; water saturation pressure parameterisation given by Murphy and Koop (2005). For comparison the homogeneous freezing of pure sulphuric acid droplets are shown from previous AIDA studies Möhler et al. (2003) along with the homogeneous freezing threshold of supercooled solution droplets Koop et al. (2000), indicated by the solid line.

ACPD
11, 11007–11038, 2011